Location of two antioxidants in oriented model membranes

Small-angle x-ray diffraction study

J. Katsaras,* R. H. Stinson,* J. H. Davis,* and E. J. Kendall‡

*Biophysics Interdepartmental Group, Department of Physics, University of Guelph, Guelph, Ontario, N1G 2W1; and ‡National Research Council Canada, Plant Biotechnology Institute, Saskatoon, Sask., Canada, S7N 0W9

ABSTRACT Small-angle x-ray diffraction has been applied in locating either butylated hydroxytoluene (BHT) or δ-tocopherol and their brominated analogues at a concentration of 40 mol% in oriented bilayers of dipalmitoylphosphatidylcholine (DPPC) or DPPC + 15 mol% cholesterol at 20°C. Phases were determined using swelling experiments with structure factors plotted in reciprocal space, creating a relatively smooth curve as the amount of water between the bilayers was changed. Continuous Fourier transforms were also calculated using sampling theory (Shannon, C. E. 1949. *Proc. Inst. Radio Engrs. NY.* 37:10–21) to further test the consistency of the phase assignments. Fourier synthesis of structure factors resulted in absolute electron density profiles for different bilayers to a resolution of 5–6 Å. In addition, difference Patterson maps were constructed to confirm the positions of the bromine atoms in the unit cell. Analysis of the data indicates the following: (*a*) The BHT molecules are dispersed throughout the alkyl-chain region in DPPC samples with and without cholesterol. (*b*) The chromanol ring of δ-tocopherol is in the vicinity of the glycerol backbone-headgroup region in samples of DPPC or DPPC + 15 mol% cholesterol. (*c*) Difference Patterson maps confirm the localization of bromine atoms in the various δ-tocopherol samples and lack of bromine localization in the various BHT samples.

INTRODUCTION

Peroxidation in a membrane or a system containing polyunsaturated fatty acids is due to the attack of a species (e.g. peroxyl radical) which is capable of abstracting a hydrogen atom from a methylene group (1). Oxidative deterioration of polyunsaturated lipids leads to a problem known as *rancidity* in foodstuffs (e.g. margarine and cooking oils). In cell membranes, lipid peroxidation causes the membrane to become less "fluid" with increasing loss of membrane integrity allowing ions such as Ca^{2+}, which normally do not cross the membrane to do so (1). In model membranes, free radicals generated by γ-irradiation promote deesterification of the fatty acids at both the 1 and 2 positions of the glycerol backbone of dipalmitoylphosphatidylcholine (DPPC). The resultant accumulation of fatty acid salts alters the bilayer's structural properties (2). Antioxidants are substances which can potentially decrease the lipid oxidation rate in membranes, polymers, and foodstuffs.

2,6-di-*tert*-butyl-4-methyl-phenol (BHT) is a very common food preservative used for its high reactivity with free radicals. It is widely used in foodstuffs ranging from dried cereal and animal foods to cooking oils and canned goods (3). In humans, BHT tends to accumulate in fat deposits and cellular membranes because it is not readily excreted or metabolized (4).

Using the stable cation radical tris (*p*-bromo-phenyl) amminium hexachloroantimonate (TBACA), Clement and Gould (3) showed that decrease of the TBACA absorbance band (centered at 725–730 nm) was linearly related to the amount of BHT present.

Physical studies in dimyristoylphosphatidylcholine (DMPC) model membrane systems have shown that BHT reduced ^{22}Na permeability in the temperature region of the gel-to-liquid–crystal phase transition, and lowered the temperatures at which the lipid chains displayed increased motional freedom (5).

Although there is still disagreement as to the biological function of tocopherols, it has been proposed (and generally accepted) that their major function is to protect fatty acids in membrane lipids from oxidative damage (6). Tocopherols are generally found in the membranes of subcellular organelles in animal and plant tissues. δ-tocopherol is a common member of this group and is reported to be the most potent antioxidant of the tocopherols (7). However, of the class of tocopherols, α-tocopherol is the most abundant and most biologically active because it is best absorbed in the mammalian gut (8).

It has generally been assumed that in lipid bilayers the chromanol ring of the tocopherols is oriented toward the water-lipid interface, while the phytyl tail is buried in the hydrophobic part of the lipid bilayer. Support for this assertion was given in a study of a 5 mol% α-tocopherol-egg phosphatidylcholine system by Perly et al. (9) using ^{13}C nuclear magnetic resonance (NMR) spectroscopy with shift and relaxation reagents, and by Srivastava et

0006-3495/91/03/645/09 $2.00

al. (10) in a 20 mol% α-tocopherol-DPPC system using electron spin resonance (ESR) and ^{13}C-NMR.

Cholesterol is a major lipid constituent in membranes of higher organisms. Although its biological function(s) is not clearly understood, it has been found to alter the physical properties of a lipid bilayer (11–13). Using a fluorescence method it was discovered that very small amounts of cholesterol incorporated into liposomes promote peroxidation (induced by iron salts and ascorbate), while greater amounts (> 5 mol%) depress it (1). The change in the liposome's susceptibility to peroxidation is probably due to structural changes induced in the bilayers by cholesterol and to cholesterol quenching some of the free radicals.

Since in any organized assembly of molecules the reactions that may occur will depend to a great extent on the positions, mobilities, and reactivities of the various reactants (membrane peroxidation being no exception), it is important to know the positions of these antioxidants in lipid bilayers in order that plausible models of protective mechanisms of lipid peroxidation can be put forth. The aim of this present work is to provide evidence for the localization of BHT and δ-tocopherol in model membrane systems of DPPC and DPPC + 15 mol% cholesterol using small-angle x-ray diffraction.

MATERIALS AND METHODS

1,2-dipalmitoyl-*sn*-glycero-3-phosphatidylcholine (DPPC) was obtained from Avanti Polar Lipids, Inc. (Birmingham, AL) and used as supplied. Lipid purity was confirmed using differential scanning calorimetry (DSC) and thin-layer chromatography (TLC, developing solvent: $CHCL_3/CH_3OH/H_2O/NH_4OH$, 58:35:5.4:1.6). DSC scans of fully hydrated liposomes revealed the gel-to-liquid–crystal phase transition at 41.2°C, having a full-width at half-maximum of 0.4°C, and TLC plates showed a single nondiffuse spot. DSC scans were obtained with a model MC-1 calorimeter (MicroCal, Inc., Amherst, MA) at a heating rate of 14.4°C/h.

2,6-di-*tert*-butyl-4-methyl-phenol (BHT, > 99%) was obtained from Aldrich Chemical Company, Inc. (Milwaukee, WI) and was recrystallized twice from ethanol. The white crystals were washed with cold ethanol after each recrystallization and then dried under vacuum for 24 h.

2,6-di-*tert*-butyl-phenol (BPH) was purchased from Fluka AG (Buchs, Switzerland) and 2,8-dimethyl-2-(4,8,12-trimethyltridecyl)-6-chromanol (δ-tocopherol) from Eastman Kodak Company (Rochester, NY). 2,6-di-*tert*-butyl-4-bromo-phenol (Br-BHT) was synthesized by the addition of bromine (1.0 M solution in CCL_4) to BPH crystals.

$$[(CH)_3C]_2C_6H_3OH \xrightarrow{Br_2} [(CH)_3C]_2C_6H_2(Br)OH. \quad (1)$$

The bromine solution was added to a round bottom flask containing the BPH crystals using a Pasteur pipette. Upon dropwise addition of the bromine solution, the brown-red color of the bromine disappeared, indicating that bromine atoms were being incorporated on the BPH rings. The round bottom flask was occasionally placed in a beaker containing hot tap water while swirling the contents. This was repeated until the color persisted. The sample was then dried using a rotary evaporator (Büchi Laboratoriums-Technik AG, Flawil, Switzerland) and the crystals placed under vacuum for 24 h at room temperature. The crystals were purified by recrystallizing twice from ethanol. The "yellowish" crystals were washed with cold ethanol after each recrystallization and finally dried under vacuum. High-resolution ^{1}H-NMR using a 400-MHz Bruker WH400 spectrometer (Bruker Spectrospin AG Zürich-Fällanden, Switzerland) indicated that > 95% of the BPH molecules had incorporated a bromine atom at the 4-position of the ring.

The synthesis of 5-bromo-δ-tocopherol was carried out as follows: one gram of δ-tocopherol was dissolved in 50 ml of diisopropyl ether (Sigma Chemical Co., St. Louis, MO). 0.2 g of ferric bromide (ALFA, Danvers, MA) and 0.4 g of bromine (Anachemica Chemicals Ltd., Montreal, Canada) were dissolved in 9 ml of 40% HBr (BDH Chemicals, Montreal, Canada) and then added to the diisopropyl ether-δ-tocopherol solution to form the reaction mixture which was constantly stirred at room temperature. After 16 h the organic phase was removed and the aqueous phase was twice extracted with 50 ml of hexane. An aliquot was removed from the combined extracts for analysis, the remainder was dried under vacuum and stored at −20°C.

Approximately 10 mg of brominated tocopherol was dissolved in perdeuterated chloroform and examined using a Bruker AM-360-WB NMR spectrometer (Bruker Spectrospin AG) operating at 360 MHz for protons. The bromination procedure resulted in the elimination of one of the aromatic proton resonances and the shift downfield by 0.3 ppm of the remaining resonance. The chemical shift of the aromatic methyl resonance at 2.12 ppm was unaffected suggesting that bromination had occurred at the 5 rather than the 7 position of the chromanol nucleus.

Brominated tocopherols were analyzed as trimethylsilyl (TMS) derivatives on a Finnigan/MAT 4500 GC-MS (Palo Alto, CA) equipped with a DB-5 (50 m × 0.32 mm i.d., 0.52 μ film thickness) capillary column. The temperature program was 100–300°C at 5°C/min. Helium was used as the carrier gas and set at a linear flow velocity of 40 cm/s when measured at 150°C. The quadrupole was operated at 70 eV and scanned from mass 43 to 650 in 1 s.

Gravimetric analysis indicated that 82% of the δ-tocopherol was recovered from the reaction mixture. Four tocopherol products were resolved during gas chromatography. 5-bromo-δ-tocopherol was the principal component ($TMS\text{-}M^+$ = 554, 85%) of the brominated tocopherol fraction. The other species present were 7-bromo-δ-tocopherol ($TMS\text{-}M^+$ = 554, 2.64%), 5-bromo-γ-tocopherol ($TMS\text{-}M^+$ = 569, 6.01%) and 5,7-di-bromo-δ-tocopherol ($TMS\text{-}M^+$ = 634, 7.23%).

Oriented bilayers were produced by a simple method developed in our lab. Two- and three-component samples were mixed in 250-ml round-bottom flasks containing methanol. The solutions were dried using a rotary evaporator at 35°C and then placed under vacuum for 24 h at room temperature. The resultant powders from solvent were placed on the outside of 30-ml Pyrex beakers (No. 1000) and pressed into thin films with the aid of a stainless steel spatula. Samples containing BHT were annealed in a 100% RH environment at 70°C, while those containing δ-tocopherol were annealed at 55°C and 100% RH environment. Anhydrous $CaSO_4$ was then added to the beakers, which were placed under vacuum for at least 24 h after which the diffraction experiments were performed. BHT samples were not placed under vacuum (to avoid sublimation) after they were oriented, but were dried under a stream of helium for 2 h. Using this simple method, we consistently obtained diffraction patterns containing 10–12 orders.

The sample holder (volume ≈ 250 cm^3) was designed to move the sample in two dimensions (horizontal and vertical with respect to the

beam) and permit the relative humidity (RH) and temperature to be adjusted and monitored. The sample holder movement was achieved by the use of stepping motors (Superior Electric Co., Bristol, CT) interfaced through a computer. The holder was positioned so that the vertical line of the x-ray beam passed through the sample tangent to the vertical curved side of the beaker. The RH was adjusted by varying the flow rate of He gas or He gas through water in a Fisher-Milligan gas washer before passage through the sample holder. Finally, the RH was monitored by a digital hygrometer (HI 8565 Stick Hygrometer; Hanna Instruments Inc., Woonsocket, RI), which has a resolution of 0.1% RH and accuracy of ±2% RH. The temperature was controlled by a Haake F_3 water bath set (Berlin, FRG) at 20°C. Small-angle x-ray (SAX) diffraction apparatus and data collection methods remained the same as those used in previous work (14).

Diffraction patterns were collected for 1,000 s. Intensities of the various diffraction peaks were determined after background subtraction. Measured intensities in general are corrected by multiplying by the square of the order number (h^2) for a powder pattern and by the order number (h) for an oriented sample (15). Our samples revealed a high degree of orientation with a total absence of wide-angle reflections with our collection geometry (i.e., linear position sensitive detector oriented to detect equitorial reflections but not the meridional wide-angle reflections). Therefore, our intensities were scaled up by a factor of h alone.

Unit cell volumes were calculated using a molecular modeling computer program (MacroModel) developed at Columbia University's chemistry department (Columbia University, New York), and average electron densities were calculated using the number of electrons and volumes of the unit cells. In previous work (14), unit cell volumes were determined from the small and wide-angle reflections. Recalculation of these systems' average electron densities using the present method, resulted in differences of ~3%. Absolute electron density distributions are obtained by using average electron densities in conjunction with either the known density of the saturated chain or headgroup region. The correct choices for these parameters were checked by the resultant water region electron density.

Phases of the various reflections were determined by the conventional swelling method (16, 17) and confirmed by the superposition of continuous transforms calculated by the use of sampling theorem (18, 19). The continuous transform, F_R, is simply constructed by laying down the function F_h [(sin π dx)/π dx] at points $x = h/d$ ($h = 0, 1, 2 \ldots . n$) with the amplitude of the function (F_h) equal to the amplitude of the structure factor at that point. The sign of the amplitude is determined by the phase. The continuous transform is then the sum of these sinc functions.

An experimental limitation lies in the fact that from a diffraction pattern the intensities are recorded without information about phase. A natural approach in this case is to investigate the result of transforming the intensity distribution (20). The Patterson function (or map), $P(u)$, of the electron density distribution, $\rho(x)$, is its auto-correlation function, i.e.,

$$P(u) = L \int_0^L \rho(x)\rho(u + x)dx \qquad (2)$$

for the one-dimensional cell of length L, where u is the fractional distance along the unit cell (21). This is a centrosymmetric function with $P(u)$ equal to the sum of the square of the atomic numbers of all atoms in the unit cell (at $u = 0$ and $u = L$) when the length of the unit cell is large. Each peak in the function will occur at values of u corresponding to plus or minus the separation of any pair of peaks in the original function $\rho(x)$. The magnitudes of the Patterson peaks will be products of the values of $\rho(x)$ of peaks in the original function which are separated by u.

The Patterson function can also be generated from diffraction data, using measured intensities I_h, and no phase information, i.e.

$$P(u) = \frac{I_0}{L} + \frac{2}{L}\sum_h I_h \cos 2\pi hu. \qquad (3)$$

Functions generated in this manner can be normalized to the values of $P(u)$ at $u = 0$ and L as described in the previous paragraph. The zeroeth order intensity (I_0) was calculated since, in any real experiment, it is impossible to differentiate it from the undiffracted radiation.

The addition of a heavy atom to two discrete locations in the unit cell will result in either intensification of existing peaks in the Patterson map if the heavy atoms localize at points initially at high electron density or the appearance of new peaks with separation governed by the location of the heavy atoms.

A difference Patterson map is a more sensitive method of locating heavy atoms and can be obtained by subtraction of diffraction data Pattersons from samples with and without the heavy atom addition. Such a difference function may contain cross-terms due to interactions between the native material and the heavy atoms (22). These cross-terms frequently cause a small peak to occur at $u = L/2$. Strong peaks in such a difference map not only indicate localization of the heavy atoms in the sample but also identify the separation of their locations. Lack of well-defined peaks results if the heavy atoms are not at discrete locations.

RESULTS AND DISCUSSION

In Fig. 1, the structure factors obtained in a series of swelling experiments for various BHT systems at 20°C are presented. We can observe that at each level of hydration, a different d-spacing is obtained permitting the sampling of the continuous Fourier transform at different points h/d. From this, it can easily be seen that both the magnitude and phase of the structure factor can change at each successive swelling state. The phases were chosen in such a manner that when plotted, the transform followed a smooth curve with changes in hydration (14, 16) and were consistent with the calculated continuous Fourier transforms (14, 16, 18, 19) of the various data sets (Fig. 2).

The structure factors in Fig. 1 seem as though they can lie on the Fourier transform of the bilayer electron density distribution (minus the water electron density) of a constant structure (23, 24). However, from Fig. 2 we can see that with swelling there seems to be a change in bilayer structure since no single transform is able to fit the data for all humidities. This same effect is seen for DPPC bilayers and is due to a decrease in bilayer thickness with increases in humidity.

In reconstructing the continuous Fourier transforms (Fig. 2), knowledge of the zeroeth order amplitude (F_0) is required. In our case, F_0 was calculated to be propor-

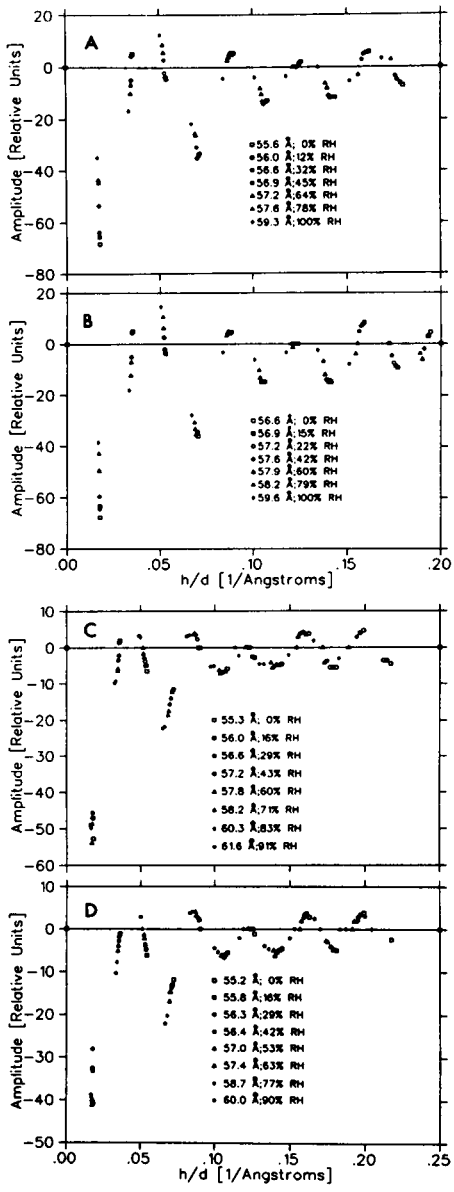

FIGURE 1 Structure factors obtained in a series of swelling experiments at 20°C for oriented multilayers of: (*a*) DPPC + 40 mol% BHT; (*b*) DPPC + 40 mol% Br-BHT; (*c*) DPPC + 15 mol% cholesterol + 40 mol% BHT; and (*d*) DPPC + 15 mol% cholesterol + 40 mol% Br-BHT.

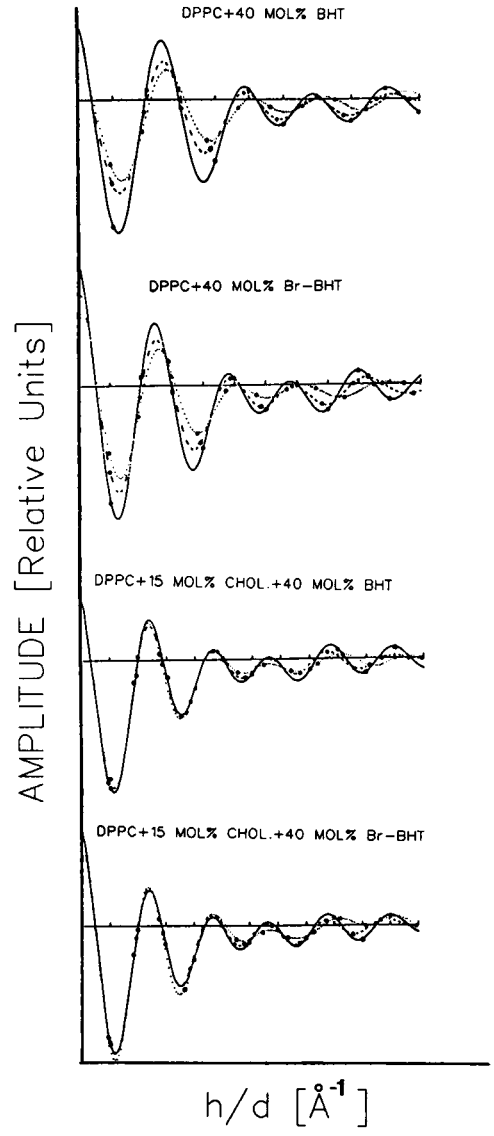

FIGURE 2 Reconstructed continuous Fourier transforms of DPPC + 40 mol% BHT (—0% RH; - - - 64% RH; ··· 100% RH), DPPC + 40 mol% Br-BHT (—0% RH; - - - 60% RH; ··· 100% RH), DPPC + 15 mol% cholesterol + 40 mol% BHT (—0% RH; - - - 60% RH; ··· 83% RH), and DPPC + 15 mol% cholesterol + 40 mol% Br-BHT (—0% RH; - - - 53% RH; ··· 90% RH).

tional to the number of electrons in the unit cell relative to water (minus-water model), and was calculated using the following expression:

$$F_0 = (\rho_{avg} - \rho_{H_2O})d, \quad (4)$$

where ρ_{avg} is the average electron density of the bilayer ρ_{H_2O} is the electron density of water. Also, F_0 remained essentially constant for the various levels of hydration since the water layers were never very thick.

From Fig. 2 we can observe that the continuous transforms of DPPC + 40 mol% BHT or Br-BHT expanded uniformly, i.e., the points at which the continuous transform crosses the reciprocal lattice axis (x-axis) moved outwards with increasing humidity, similar to the case of DPPC alone (14, 23). This implies that with increasing hydration there is a decrease in the thickness

of the bilayer (14, 23). Comparison of electron density distributions of hydrated vs. nonhydrated DPPC + 40 mol% BHT or Br-BHT samples (not shown) showed a similar reduction of bilayer thickness (from ~48 to ~44 Å) with increases in hydration. Samples of DPPC + 40 mol% BHT or Br-BHT which contained 15 mol% cholesterol, also exhibited changes in the continuous transform with increasing humidity, but not to the same extent as those samples for which cholesterol was not incorporated. Comparison of the electron density distributions of the hydrated vs. nonhydrated cholesterol containing samples (not shown) showed only a slight decrease in bilayer thickness (from ~50 to ~49 Å peak to peak), while experiencing an increase in the water layer of ~7 Å. These latter samples seem to behave in a similar fashion to DPPC + 40 mol% 2-bromo palmitic acid bilayers at 20°C (14). Electron density profiles of oriented egg lecithin bilayers also show a reduction in bilayer thickness as humidity is increased (23). However, upon the addition of 40 mol% cholesterol, electron density distributions calculated from the data to ~6.5 Å spacing showed that the bilayer thickness remained relatively constant with swelling (24).

The principal goal of an x-ray diffraction experiment is the computation of the electron density function and its interpretation in terms of the distribution and location of the component molecules. This is done by obtaining values for all structure factors (magnitude and phase) and performing a Fourier synthesis. The results of the Fourier synthesis for the various lipid-BHT samples are presented in Fig. 3. In Fig. 3 *a* the electron density distributions of DPPC + 40 mol% BHT (avg. $\rho[x] = 0.354$ electrons/Å^3) and DPPC + 40 mol% Br-BHT (avg. $\rho[x] = 0.364$ electrons/Å^3) at 100% RH and 20°C are contrasted on an absolute scale. From the comparison, we can observe that the profiles are similar in the water and glycerol backbone-headgroup regions, but differ markedly throughout the region of the hydrocarbon tails. This implies that the bromines and thus, the BHT molecules are not localized but are distributed in the hydrophobic part of the bilayer. In Fig. 3 *b*, comparison of DPPC + 15 mol% cholesterol + 40 mol% BHT (avg. $\rho[x] = 0.354$ electrons/Å^3) and DPPC + 15 mol% cholesterol + 40 mol% Br-BHT (avg. $\rho[x] = 0.365$ electrons/Å^3) bilayers, yielded similar results.

These results are a departure from similar types of experiments where the halogen atoms are well localized (14, 25, 26). In such cases of localization, the interpretation of the data can be simplified. This was demonstrated by Franks et al. (25) using dimyristoyl lecithin (DMPC) with 40 mol% cholesterol or cholesterol analogues halogenated at the C-26 position. Because the C-26 position of cholesterol is well localized near the

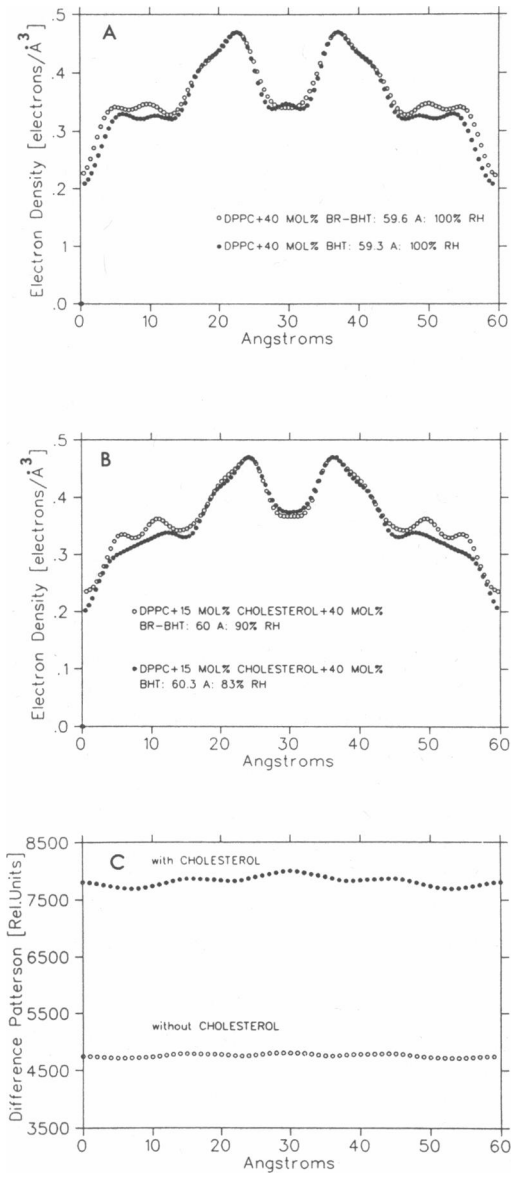

FIGURE 3 Absolute electron density profiles showing differences between: (*a*) DPPC + 40 mol% BHT and DPPC + 40 mol% Br-BHT; (*b*) DPPC + 15 mol% cholesterol + 40 mol% BHT and DPPC + 15 mol% cholesterol + 40 mol% Br-BHT; and (*c*) their respective difference Patterson functions.

center of the bilayer, the difference electron density profile resulted in a single peak indicating the location of the halogen atoms. Another experiment performed by Katsaras and Stinson (14) using DPPC and 40 mol% palmitic acid and 2-bromo palmitic acid, showed localization of the bromine atoms in the vicinity of the glycerol backbone. In this experiment, the bromine atoms from opposing leaflets are not in close proximity to each

other, and thus two peaks associated with the locations of the bromines are observed.

To derive an electron density distribution we must carry out a Fourier synthesis of the structure factors. However, because intensities are recorded without phase information it was decided to also use a technique that is independent of phase. The transformation operation applied to the intensities alone is known as a Patterson synthesis. In Fig. 3 *c* we present difference Patterson maps of the original DPPC + 40 mol% BHT bilayers and their heavy atom derivatives, with and without cholesterol. The difference Patterson is a sensitive method of identifying the positions of heavy elements, but in neither of the two BHT cases did the difference Pattersons exhibit strong peaks. From this result we can conclude that the bromine atoms and therefore the BHT molecules are not localized at any single site in the bilayer, whether or not cholesterol is present.

The indication that the BHT molecules are not localized in any one part of the bilayer (at these mol%'s) is not surprising because the hydroxyl group of a BHT molecule is well shielded by the two-*tert*-butyl groups with the result that its polar characteristics are reduced (27). Chaykowski et al. (28), using ESR in model membrane systems (DMPC, DPPC), proposed that a greater increase in fatty acyl chain disorder (or dynamics) occurs when molecules are intercalated near the lipid-water interface rather than when placed in the middle of the bilayer. In terms of this "gradient" model, it was found that 4-*tert*-butylphenol was more effective than 2-*tert*-butylphenol in increasing fatty acyl chain movement. This was attributed to the 4-*tert*-butylphenol orienting itself with its hydroxyl group at the interface and its butyl group in the bilayer.

We performed experiments similar to the ones using BHT with various δ-tocopherol systems. The methods of experimentation and analysis for these systems were identical to those which contained BHT. In Figs. 4 and 5 the structure factors for DPPC + 40 mol% δ-tocopherol, with and without cholesterol are plotted. Samples of DPPC + 40 mol% δ-tocopherol and Br-δ-tocopherol contained a nonlamellar reflection in the region of the second order at relative humidities of $<70\%$. The nonbrominated δ-tocopherol sample containing 15 mol% cholesterol, also exhibited this nonlamellar reflection at RH values of $<55\%$ but was absent in its brominated analogue. Since we could not arrive at a consistent explanation for these nonlamellar reflections (e.g., aggregation of δ-tocopherol at low levels of hydration), we calculated continuous Fourier transforms (Fig. 6) and absolute electron density distributions (Fig. 7) with only those samples that did not contain the anomalous reflection.

Absolute electron density profiles for the various

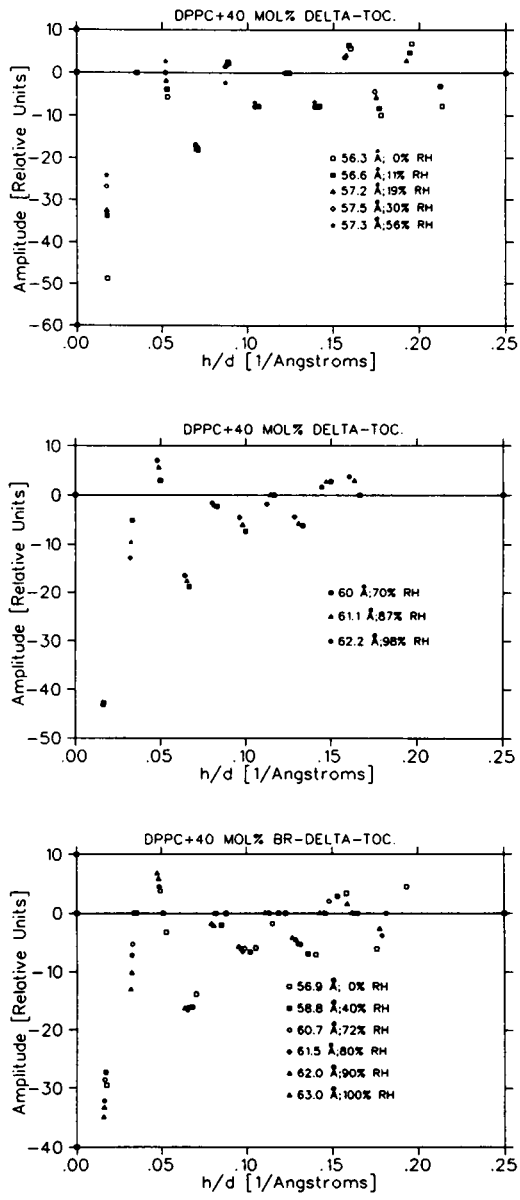

FIGURE 4 Structure factors obtained in a series of swelling experiments at 20°C for oriented multilayers of DPPC + 40 mol% δ-tocopherol or 40 mol% Br-δ-tocopherol.

δ-tocopherol systems, derived from the continuous transforms (Fig. 6), are shown in Figs. 7, *a* and *b*. In Fig. 7 *a*, the electron density maps of DPPC + 40 mol% δ-tocopherol (avg. $\rho[x] = 0.350$ electrons/Å^3) and DPPC + 40 mol% Br-δ-tocopherol (avg. $\rho[x] = 0.360$ electrons/Å^3) at 20°C are compared. The comparison indicates that the two samples are similar in the water and hydrocarbon tail regions, but differ substantially in the regions of the glycerol backbone and headgroup. Similar results were obtained when samples of nonbrominated

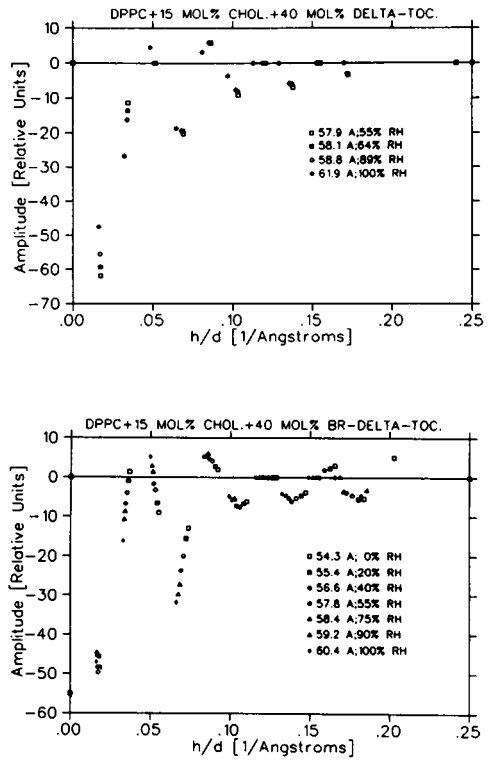

FIGURE 5 Structure factors obtained in a series of swelling experiments at 20°C for oriented multilayers of DPPC + 15 mol% cholesterol + 40 mol% δ-tocopherol or 40 mol% Br-δ-tocopherol.

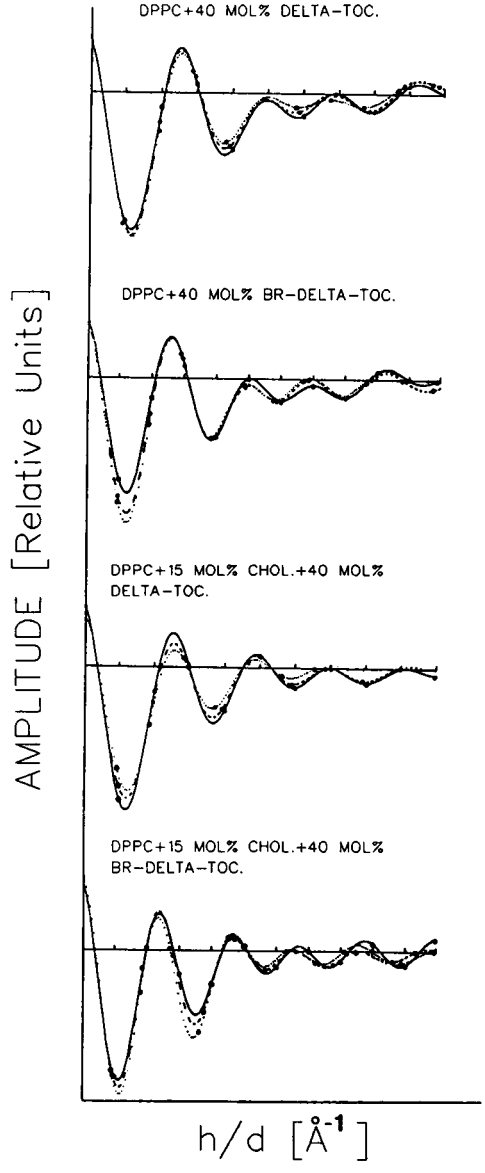

FIGURE 6 Reconstructed continuous Fourier transforms of DPPC + 40 mol% δ-tocopherol (−70% RH; - - - 87% RH; ··· 98% RH), DPPC + 40 mol% Br-δ-tocopherol (−70% RH; - - - 90% RH; ··· 100% RH), DPPC + 15 mol% cholesterol + 40 mol% δ-tocopherol (−55% RH; - - - 89% RH; ··· 100% RH), and DPPC + 15 mol% cholesterol + 40 mol% Br-δ-tocopherol (−0% RH; - - - 55% RH; ··· 100% RH).

δ-tocopherol containing 15 mol% cholesterol (avg. $\rho[x]$ = 0.350 electrons/Å^3) are contrasted with their brominated analogues (avg. $\rho[x]$ = 0.360 electrons/Å^3), as shown in Fig. 7 *b*.

Their results indicate relatively good localization of the attached bromines as did similar previous experiments (14, 25, 26). Using a DPPC + 40 mol% palmitic acid system at 20°C, we were able to show that the bromine attached to the 2 position of the fatty acid was extremely well localized in the vicinity of the glycerol backbone (14). In this present case, we find that the bromine (which is attached to the 5 position of the chromanol moiety) is distributed over a somewhat broader region in the glycerol backbone-headgroup region regardless of the presence or absence of cholesterol (Fig. 7, *a* and *b*). The weak localization of the δ-tocopherol molecules observed in the DPPC bilayers may also occur in biological membranes. However, the fact that we used a saturated gel-phase lipid and 40 mol% δ-tocopherol may have contributed to this distribution.

To further test the correctness of the electron density distributions we calculated difference Patterson maps in the same manner as we did for the various BHT samples (Fig. 7 *c*). However, in contrast to the BHT difference Patterson maps, the δ-tocopherol difference maps contain strong peaks due to the bromine atoms. The peaks of the Patterson function are located in positions corresponding to separation of peaks in the electron density function, but are broader. The width of a Patterson peak is equal to the sum of the widths of the two peaks in the electron density function. The bromine peaks in the

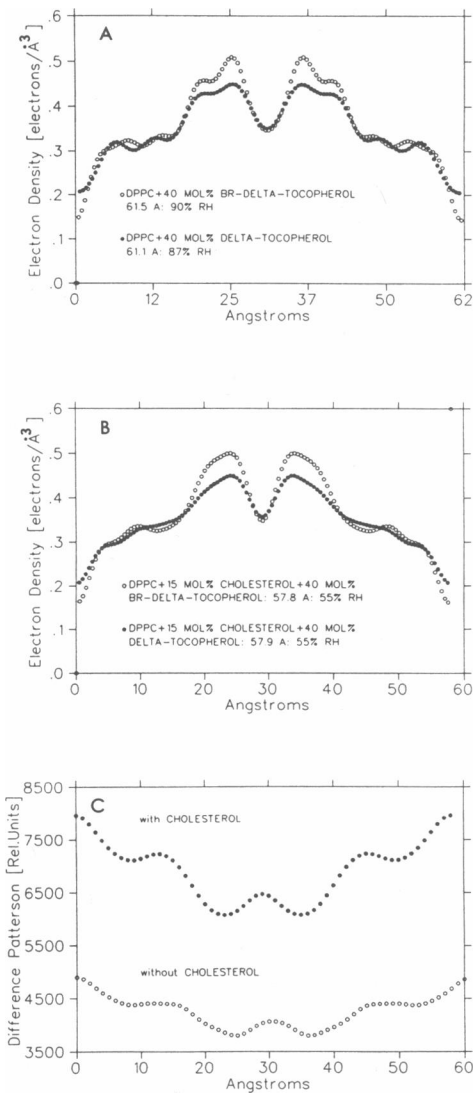

FIGURE 7 Absolute electron density profiles showing differences between: (*a*) DPPC + 40 mol% δ-tocopherol and DPPC + 40 mol% Br-δ-tocopherol; (*b*) DPPC + 15 mol% cholesterol + 40 mol% δ-tocopherol and DPPC + 15 mol% cholesterol + 40 mol% Br-δ-tocopherol; and (*c*) their respective difference Patterson maps.

difference Patterson maps are centered at ~15 Å with widths of ~16 Å. This is consistent with the appearance of regions of additional intensity in the electron density distributions of the various brominated δ-tocopherol samples which have widths of ~9 Å and centers separated by ~15 Å.

These results are in general agreement with studies using ^{13}C-NMR, and various systems containing α-tocopherol. Perly et al. (9) using ^{13}C-NMR and 5 mol% α-tocopherol in egg lecithin concluded that in small unilamellar vesicles, α-tocopherol distributes itself uniformly between the inner and outer monolayers. In addition, they found that the α-tocopherol molecules had their phytyl tails embedded in the lipid bilayer and their phenolic hydroxyl groups located in the vicinity of the lipid's phosphate moiety. Srivastava et al. (10) using ESR, ^{13}C-NMR and a 20 mol% α-tocopherol system in DPPC vesicles, concluded that the α-tocopherol's hydroxyl group was capable of forming hydrogen bonds with the oxygen atoms associated with the DPPC's phosphate region or with water molecules at the lipid-water interface.

Electron density profiles (not shown) with 95% confidence envelopes have been created for various samples. In all cases the envelopes are close to the values shown in Figs. 3 and 7 and lie within the circles used to map out the electron density profiles. These confidence limit profiles were calculated using the equations described by Franks and Lieb (29). We start with the measured intensities (gross counts minus background) whose uncertainties are determined by counting statistics. Very strong diffraction peaks frequently contained about one million counts with a 95% confidence of ~0.5%. The weakest reflections, at the other extreme, would have only a few hundred counts with corresponding uncertainties in the range of 30–45%. The structure factors calculated from the measured intensities are normalized so that the correct absolute electron density is obtained directly from their Fourier transform. The uncertainties in these structure factors (δF_h) will be, on a relative basis, one half of those for the corresponding intensities. The 95% uncertainty limits of $\rho(x)$ are then calculated from:

$$\delta\rho(x) = \frac{2}{d}\left[\sum_{h=1}^{h\,max} (\delta F_h)^2 \cos^2\left(\frac{2\pi hx}{d}\right)\right]^{1/2}. \quad (5)$$

This is the equation used by Franks and Lieb (29) with the addition of the "*d*" under the leading 2. This is necessary for the calculation of absolute electron densities rather than the relative values used in their paper. In our calculations the largest $\delta\rho(x)$ obtained was ± 0.0035 at a $\rho(x)$ of 0.143 and the smallest was ± 0.0013 at $\rho(x)$ = 0.405.

CONCLUSION

SAX diffraction patterns containing up to 12 orders were obtained for various oriented DPPC bilayers containing BHT or δ-tocopherol (and their brominated analogues) with and without cholesterol.

High-resolution electron density distributions (5–6 Å) of DPPC + 40 mol% BHT or 40 mol% Br-BHT in the presence or absence of cholesterol revealed that the

BHT molecules are not localized, but distributed throughout the hydrophobic region of the bilayer. In contrast, the electron density distributions of bilayers made up of DPPC + 40 mol% δ-tocopherol or Br-δ-tocopherol with and without cholesterol, located the bromines (thus the 5 position of the chromanol groups) in the vicinity of the glycerol backbone-headgroup region.

To confirm the validity of these profiles, we calculated phase-independent maps known as difference Pattersons. The interpretations of these maps are consistent with the results indicated by the electron density profiles.

We would like to thank Denis Langlais, Scott Prosser, and Professors I. K. MacKenzie and K. R. Jeffrey.

This research was supported by a grant from the Natural Sciences and Engineering Research Council of Canada. Dr. Katsaras was partially supported by a scholarship through the provincial government of Ontario.

Received for publication 21 June 1990 and in final form 25 October 1990.

REFERENCES

1. Halliwell, B., and J. M. C. Gutteridge. 1985. Free Radicals in Biology and Medicine. Clarendon Press, Oxford.
2. Katsaras, J., R. H. Stinson, E. J. Kendall, and B. D. McKersie. 1986. Structural simulation of free radical damage in a model membrane system: a small-angle x-ray diffraction study. *Biochim. Biophys. Acta.* 861:243–250.
3. Clement, N. R., and J. M. Gould. 1980. Quantitative detection of hydrophobic antioxidants such as butylatedhydroxytoluene and butylatedhydroxyanisole in picomole amounts. *Anal. Biochem.* 101:299–304.
4. Chen, C., and Y-S. Shaw. 1974. Cyclic metabolic pathway of a butylated hydroxytoluene by rat liver microsomal fractions. *Biochem. J.* 144:497–501.
5. Singer, M., and J. Wan. 1977. Interaction of butylated hydroxytoluene (BHT) with phospholipid bilayer membranes: effect on ^{22}Na permeability and membrane fluidity. *Biochem. Pharmac.* 26:2259–2268.
6. Burton, G. W., and K. U. Ingold. 1986. Vitamin E: application of the principles of physical organic chemistry to the exploration of its structure and function. *Acc. Chem. Res.* 19:194–201.
7. Stecher, P. G. editor. 1968. The Merck Index. 8th ed. Merck and Co., Inc. Rahway, NJ.
8. Burton, G. W., and K. U. Ingold. 1981. Autoxidation of biological molecules. 1. The antioxidant activity of vitamin E and related chain-breaking phenolic antioxidants *in vitro*. *J. Am. Chem. Soc.* 103:6472–6477.
9. Perly, B., I. C. P. Smith, L. Hughes, G. W. Burton, and K. U. Ingold. 1985. Estimation of the location of natural α-tocopherol in lipid bilayers by ^{13}C-NMR spectroscopy. *Biochim. Biophys. Acta.* 819:131–135.
10. Srivastava, S., R. S. Phadke, G. Govil, and C. N. R. Rao. 1983. Fluidity, permeability and antioxidant behaviour of model membranes incorporated with α-tocopherol and vitamin E acetate. *Biochim. Biophys. Acta.* 734:353–362.
11. Vist, M. R., and J. H. Davis. 1990. Phase equilibria of cholesterol/dipalmitoylphosphatidylcholine mixtures: ^2H nuclear magnetic resonance and differential scanning calorimetry. *Biochemistry.* 29:451–464.
12. Finean, J. B. 1990. Interaction between cholesterol and phospholipid in hydrated bilayers. *Chem. Phys. Lipids.* 54:147–156.
13. Hjort Ipsen, J., G. Karlström, O. G. Mouritsen, H. Wennerström, and M. J. Zuckermann. 1987. Phase equilibria in the phosphatidylcholine-cholesterol system. *Biochim. Biophys. Acta.* 905:162–172.
14. Katsaras, J., and R. H. Stinson. 1990. High-resolution electron density profiles reveal influence of fatty acids on bilayer structure. *Biophys. J.* 57:649–655.
15. Stinson, R. H., and J. M. Boggs. 1989. Interdigitated lipid bilayers of long acyl species of cerebroside sulfate. An x-ray diffraction study. *Biochim. Biophys. Acta.* 986:234–240.
16. Franks, N. P., and W. R. Lieb. 1981. X-Ray and neutron diffraction studies of lipid bilayers. *In* Liposomes: From Physical Structure to Therapeutic Applications. C. G. Knight, editor. Elsevier/North-Holland Biomedical Press, Amsterdam. 243–272.
17. Worthington, C. R., and T. J. McIntosh. 1973. Direct determination of the electron density profile of nerve myelin. *Nat. New Biol.* 245:97–99.
18. Shannon, C. E. 1949. Communication in the presence of noise. *Proc. Inst. Radio Engrs. NY.* 37:10–21.
19. Sayre, D. 1952. Some implications of a theorem due to Shannon. *Acta Crystallogr. Sect. B.* 5:843.
20. Lipson, H., and C. A. Taylor. 1958. Fourier Transforms and X-Ray Diffraction. G. Bell and Sons, Ltd., London.
21. Sherwood, D. 1976. Crystals, X-Rays and Proteins. Longman Group Ltd., London.
22. Ramachandran, G. N., and R. Srinivasan. 1970. Fourier Methods in Crystallography. John Wiley and Son, Inc., New York.
23. Torbet J., and M. H. F. Wilkins. 1976. X-Ray diffraction studies of lecithin bilayers. *J. Theor. Biol.* 62:447–458.
24. Franks, N. P. 1976. Structural analysis of hydrated egg lecithin and cholesterol bilayers. I. X-Ray diffraction. *J. Mol. Biol.* 100:345–358.
25. Franks, N. P., T. Arunachalam, and E. Caspi. 1978. A direct method for the determination of membrane electron density profiles on an absolute scale. *Nature (Lond.).* 276:530–532.
26. McIntosh, T. J., and P. W. Holloway. 1987. Determination of the depth of bromine atoms in bilayers formed from bromolipid probes. *Biochemistry.* 26:1783–1788.
27. Law, P., S. D. Campbell, J. R. Lepock, and J. Kruuv. 1986. Effects of butylated hydroxytoluene on membrane lipid fluidity and freeze-thaw survival in mammalian cells. *Cryobiology.* 23:317–322.
28. Chaykowski, F. T., J. K. S. Wan, and M. A. Singer. 1979. Interaction of small molecules with phospholipid bilayer membranes: a spin label study. *Chem. Phys. Lipids.* 23:111–123.
29. Franks, N. P., and W. R. Lieb. 1979. The structure of lipid bilayers and the effects of general anaesthetics. An x-ray and neutron diffraction study. *J. Mol. Biol.* 13:469–500.